LETTER

doi:10.1038/nature11653

Revealing the quantum regime in tunnelling plasmonics

Kevin J. Savage[1], Matthew M. Hawkeye[1], Rubén Esteban[2], Andrei G. Borisov[2,3], Javier Aizpurua[2] & Jeremy J. Baumberg[1]

When two metal nanostructures are placed nanometres apart, their optically driven free electrons couple electrically across the gap. The resulting plasmons have enhanced optical fields of a specific colour tightly confined inside the gap. Many emerging nanophotonic technologies depend on the careful control of this plasmonic coupling, including optical nanoantennas for high-sensitivity chemical and biological sensors[1], nanoscale control of active devices[2–4], and improved photovoltaic devices[5]. But for subnanometre gaps, coherent quantum tunnelling becomes possible and the system enters a regime of extreme non-locality in which previous classical treatments[6–14] fail. Electron correlations across the gap that are driven by quantum tunnelling require a new description of non-local transport, which is crucial in nanoscale optoelectronics and single-molecule electronics. Here, by simultaneously measuring both the electrical and optical properties of two gold nanostructures with controllable subnanometre separation, we reveal the quantum regime of tunnelling plasmonics in unprecedented detail. All observed phenomena are in good agreement with recent quantum-based models of plasmonic systems[15], which eliminate the singularities predicted by classical theories. These findings imply that tunnelling establishes a quantum limit for plasmonic field confinement of about $10^{-8}\lambda^3$ for visible light (of wavelength λ). Our work thus prompts new theoretical and experimental investigations into quantum-domain plasmonic systems, and will affect the future of nanoplasmonic device engineering and nanoscale photochemistry.

Subwavelength metallic structures can concentrate light into nanoscale dimensions well below the diffraction limit[16] owing to reduced field penetration through a dense electron sea. Nanocavities formed inside a nanogap control the coupling of localized plasmons, thus allowing cavity-tuning[6–8] targeted to desirable applications that exploit the enhanced optical fields. But as the cavity gaps shrink to atomic length scales, quantum effects emerge and standard classical approaches to describe the optics of these systems fail. One effect of confining electronic wavefunctions to small metallic nanoparticles is to slightly modify the screening that tunes the plasmons[17]. However, tunnelling plasmonics in the quantum regime has more profound effects that cannot be explained through hydrodynamic models that account for quantum effects through smearing of the electronic localization[18]. Recent theories show that quantum tunnelling across the cavity strongly modifies the optical response[19,20], but computational limits restrict these quantum simulations to very small systems below a few nanometres in size. Furthermore, the extreme difficulty of creating and probing subnanometre cavities has limited experimental investigations of plasmonics in the quantum regime. Top-down and self-assembly nanofabrication achieves gaps as small as 0.5 nm between plasmonic nanoparticles[21,22], but these fail to reach the quantum tunnelling regime. Small cavities are also accessed in scanning tunnelling microscopes and electro-migrated break-junctions which show optical mixing, emission and rectification phenomena[23–26], but the effect of quantum tunnelling on optical plasmon coupling across subnanometre cavities remains unexplored. Here we present broadband optical spectra that probe dynamically controlled plasmonic cavities and reveal the onset of quantum-tunnelling-induced plasmonics in the subnanometre regime.

Two gold-nanoparticle-terminated atomic force microscope (AFM) tips are oriented tip-to-tip (Fig. 1a). The tip apices define a cavity supporting plasmonic resonances created via strong coupling between localized plasmons on each tip[7,27]. This dual AFM tip configuration provides multiple advantages. First, independent nanometre-precision movement of both tips is possible with three-axis piezoelectric stages. Second, conductive AFM probes provide direct electrical connection to the tips, enabling simultaneous optical and electrical measurements. Third, the tips are in free space and illuminated from the side in a dark-field configuration (Fig. 1b, c and Supplementary Information). This arrangement provides (for the first time, to our knowledge) background-free broadband spectroscopic characterization of the tip–tip plasmonic nanocavity throughout the subnanometre regime. A supercontinuum laser (with polarization parallel to the tip–tip axis) is used as an excitation source, providing high-brightness illumination over a wide wavelength range (450–1,700 nm) and reducing integration times to a few milliseconds. The tips are aligned using a recently developed electrostatic-force technique[28]. The inter-tip separation d is initially set to 50 nm and then reduced while recording dark field scattering spectra and direct currents simultaneously.

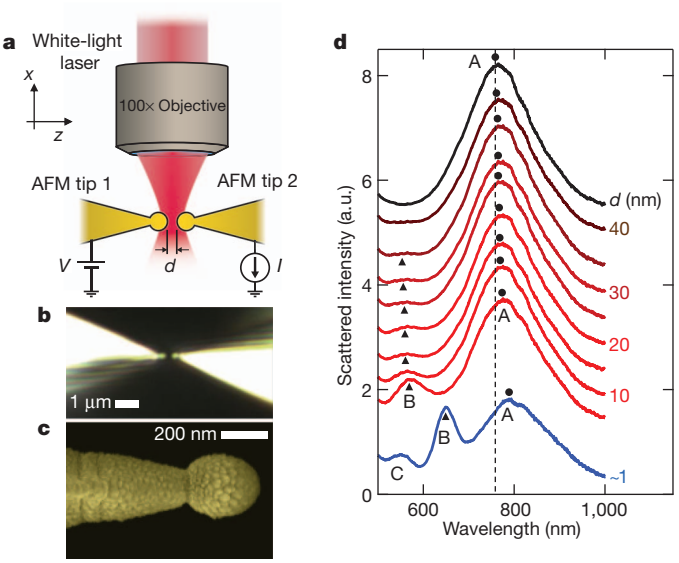

Figure 1 | Formation and characterization of a nanoscale plasmonic cavity. **a**, Scheme for simultaneous optical and electrical measurements of plasmonic cavity formed between two Au-coated tips, shown in dark-field microscope images (**b**) and false-colour scanning electron microscope image (**c**) of a typical tip, end radius $R = 150$ nm. **d**, Measured dark field scattering spectra from one inter-tip cavity at different cavity widths d. Plasmonic cavity resonances are labelled A–C.

[1]Nanophotonics Centre, Cavendish Laboratory, University of Cambridge, Cambridge CB3 0HE, UK. [2]Material Physics Center CSIC-UPV/EHU and Donostia International Physics Center DIPC, Paseo Manuel de Lardizabal 5, 20018 Donostia-San Sebastián, Spain. [3]Institut des Sciences Moléculaires d'Orsay – UMR 8214, CNRS-Université Paris Sud, Bâtiment 351, 91405 Orsay Cedex, France.

Each piezoelectric scan investigates three interaction regimes: capacitive near-field coupling ($50\,\text{nm} > d > 1\,\text{nm}$), quantum regimes ($1\,\text{nm} > d > 0\,\text{nm}$) and physical contact with conductive coupling ($d \leq 0\,\text{nm}$). Crucially, this set-up allows us to resolve the gradual transition between each regime dynamically. The measured dark-field scattering spectra (Fig. 1d) within the capacitive regime ($d \approx 40\,\text{nm}$) show a single plasmonic scattering peak centred near $\lambda = 750\,\text{nm}$ (mode A). As d is reduced, this peak redshifts owing to increasing near-field interactions between the tip plasmons. As the cavity shrinks below 20 nm, a second scattering peak emerges at shorter wavelengths (mode B, $\lambda = 550\,\text{nm}$) and quickly increases in intensity. Modes A and B smoothly redshift until an estimated separation $d = 5\,\text{nm}$, whereupon attractive inter-tip forces overwhelm the AFM-cantilever restoring force and snap the tips into close proximity[29]. However no current flow is detectable because this snap-to-contact point does not coincide with conductive contact and the metal surfaces remain separated. Snap-to-contact reduces d to $\sim$1 nm, significantly increasing the plasmonic interaction and dramatically changing the plasmonic scattering resonances (blue curve, Fig. 1d). This increased coupling further redshifts modes A and B and reveals a new higher-order resonance (mode C) at $\lambda = 540\,\text{nm}$. After snap-to-contact, increased piezoelectric displacement applies an additional compressive force (0.1 nN per nm of displacement), pushing the tips into closer proximity. After 11.4 nN of force in this run, current flow is detected through the tips, indicating metal-to-metal surface contact. Detailed calculations confirm that the coupled plasmonic modes observed are tightly confined in the nanocavity (see below, and Supplementary Information).

Simultaneously monitoring the optical and electrical properties during approach reveals in detail the plasmon evolution through the subnanometre regime (Fig. 2a–c). As the applied force increases and d is reduced, all three modes redshift and modes A and B weaken while mode C intensifies. The line widths of modes A and B decrease in concert with this reduced scattering strength while mode C broadens owing to increased scattering loss. These spectral changes are well-reproduced by simulations that include quantum tunnelling (Fig. 2d). The calculations employ the quantum corrected model (QCM), a new approach derived from time-dependent density-functional theory that allows incorporation of quantum coherent electron tunnelling into a classical electromagnetic framework to treat large plasmonic systems (Supplementary Information)[15]. For $d \gtrsim 0.4\,\text{nm}$, plasmon interactions are consistent with the classical picture (Fig. 2e), accounting for rapidly increasing redshifts as d decreases and a transfer of oscillator strength from modes A and B to mode C, as observed. Although these higher-order coupled modes have been predicted theoretically[7,8], they are clearly revealed here dynamically on approach.

At an applied force greater than 8 nN, a new regime is seen that deviates strongly from the classical predictions; modes A and B are now shifting back to shorter wavelengths instead of redshifting divergently. This crossover is clearly seen in the QCM simulations at $d \approx 0.31\,\text{nm}$ (Fig. 2d). The quantum and classical predictions diverge at this crossover point (d_{QR}) because the plasmon interactions enter the quantum regime (QR) when d is sufficiently small to support a critical electron tunnelling rate between the surfaces. Although electron confinement within each tip is minimally affected at this separation, the quantum tunnelling here dramatically modifies the correlations between electronic fluxes[15]. The net result is that quantum-tunnelling charge transfer screens the localized plasmon surface charge, decreasing the enhanced fields and reducing plasmonic coupling. For $d < d_{QR}$, this quantum tunnelling increases exponentially and quickly dominates, creating charge-transfer plasmon modes that blueshift towards $d = 0$.

The redshift-to-blueshift crossover corresponds to the threshold at which quantum-tunnelling charge reduction starts balancing the near-field capacitive coupling. We can estimate d_{QR} roughly by considering charge tunnelling between the surfaces over an optical half-cycle. In the simplest model of a rectangular barrier, when half the plasmon charge is transferred across the junction for a critical gap ($\tilde{d}_{QR}$) marking the onset of the quantum regime, $\tilde{d}_{QR} = \ln(3q\lambda\alpha/2\pi)/2q$, where q is the semiclassical electron tunnelling wavenumber, λ is the optical plasmon wavelength and $\alpha \approx 1/137$ is the fine structure constant (see Supplementary Information). At $\lambda = 850\,\text{nm}$, this zeroth-order calculation gives $\tilde{d}_{QR} = 0.16\,\text{nm}$. Full calculations show that at $d_{QR} \approx 0.31\,\text{nm}$ sufficient screening has already developed via the quantum transport to overcome the increasing charge build-up, consistent with the estimate for $\tilde{d}_{QR}$ above. Realistically including the coherent quantum transport strongly enhances the tunnelling rate compared to the estimate for the square tunnel barrier used above, increasing the distance at which tunnelling plasmonics takes over, and dictating the emergence of quantum-tunnelling charge-transfer plasmons.

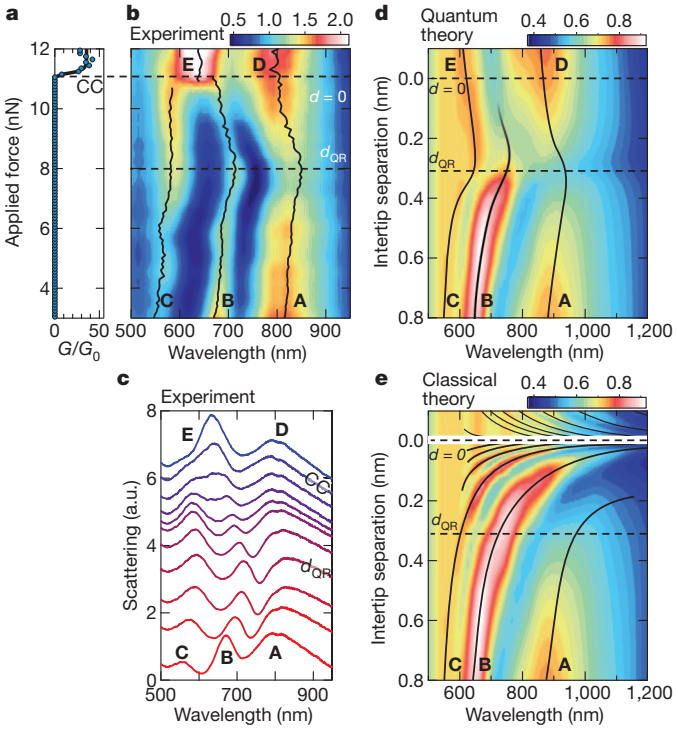

Figure 2 | Onset of quantum tunnelling in sub-nm plasmonic cavities. **a**, **b**, Simultaneously measured electrical conductance (**a**) and dark-field optical back-scattering (**b**) with increasing force applied to the inter-tip cavity after snap-to-contact. Conductive contact (CC) indicates $d = 0$, with onset of quantum regime at d_{QR}. Lines track peak positions. **c**, Selected experimental spectra from the last 1 nm to contact in **b**, shown vertically shifted. **d**, Theoretical total scattering intensity from a tip–tip system incorporating quantum mechanical tunnelling. The threshold (at d_{QR}) indicates where quantum-tunnelling-induced charge screening overcomes the near-field capacitive interaction between plasmons. **e**, Theoretical scattering intensity as in **d** but using purely classical calculations.

After conductive contact ($d = 0$), when the conductance G first jumps above $G_0 = 2e^2/h$ (here e is the charge on the electron), two scattering peaks are observed—modes D (800 nm) and E (640 nm). Tracking modes A, B and C through the quantum regime as $d \to 0$ shows the gradual nature of this contact transition, in marked contrast to the singular transition predicted classically (Fig. 2e), where a dense continuum of modes builds up in the touching limit[7,8]. At d_{QR} mode A weakens sharply, before a new peak appears which blueshifts and intensifies towards conductive contact. While mode B weakens at d_{QR}, mode C strengthens as predicted by the QCM. In both theory and experiment, modes B and C are replaced by mode E at contact. Spectra and conductance change minimally for increasing contact force after conductive contact, indicating a stable final contact. Experiments on a variety of tips show repeatable crossover behaviour at $d < d_{QR}$ (see Supplementary Information), which forms an optical fingerprint of the new tunnelling plasmonics regime.

To understand plasmon evolution through the quantum regime, the cavity field-distribution is calculated within the QCM accounting for quantum effects (Fig. 3). This allows us to construct a model of tunnelling plasmonics (Fig. 3a). For $d > d_{QR}$ (I in Fig. 3a), spectra are dominated by the near-field interaction of the cavity-localized surface charges and plasmons couple according to classical models. Once $d \approx d_{QR}$, the system enters the quantum regime (II in Fig. 3a) and tunnelling opens a conductance channel between the surfaces, modifying the plasmon charge distribution, screening the electric field and reducing the interaction strength. The tunnelling (which is strongly concentrated across the thinnest barrier region) pinches off the field distribution in the centre of the gap, systematically separating the single field lobe into two lobes in the crevices on either side of the neck (Fig. 3b). As d is reduced further (III in Fig. 3a, b), these quantum-tunnelling charge-transfer modes concentrated around the contact crevices blueshift as their apices become blunter. Around d_{QR}, the mode strengths of A and B reach their weakest values because the tunnelling increases sufficiently to screen the charges across the gap, but cannot provide sufficient current to drive the charge-transfer modes into the crevices. Hence at this point the total separated charge localized to the contact region decreases, reducing the optical cross-section.

The onset of quantum tunnelling fundamentally limits optical field confinement in plasmonic nanocavities. The plasmonic surface charge between two spherical surfaces of curvature R is confined laterally to $w \approx \sqrt{Rd}$ (ref. 7), as confirmed by our simulations (Fig. 3c). However, quantum tunnelling limits w to $w_{QL} \geq \sqrt{Rd_{QR}}$. Further reducing d rapidly increases the mode spatial width, as the surfaces are quantum-mechanically blurred at this microscopic scale. The tunnelling plasmonics regime thus represents the quantum limit of compression of light that is plasmonically squeezed into a nanogap, as verified in our experiments and QCM calculations. The quantum-limited mode volume can be approximated as $V_{min} = \pi R d_{QR}^2/4$, which is estimated to be $V_{min} \approx 1.7 \times 10^{-8}\lambda^3$ in our experiments at $\lambda = 850$ nm (mode A at d_{QR}). As this limit for plasmonics is six orders of magnitude smaller than the tightest field confinement observed in photonic crystal cavities, it still offers unprecedented opportunities for directly visualizing atomic-scale and molecular processes with electronvolt-scale photons.

These experimental and theoretical investigations of plasmonic interactions in subnanometre metal cavities demonstrate that quantum mechanics is already important at the 0.3-nm scale at which tunnelling plasmonics starts to dominate. This understanding is crucial for describing light–matter interactions down to the atomic scale. Stabilizing single-atom contacts or wires will give direct plasmonic access to the quantum transport regime around $1G_0$ (ref. 30). Our work opens up new prospects, such as directing and controlling the chemistry of single molecules within nanogaps (for example, for enhanced photocatalysis), exploiting single-molecule plasmon-assisted transport across nanogaps (for example, for single-molecule electronics), investigating extreme nonlinear interactions and accessing photo-electrochemistry on the subzeptolitre scale.

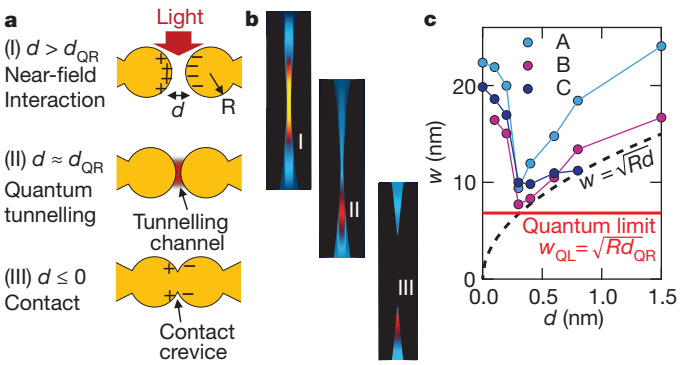

Figure 3 | Evolution of the plasmonic modes through the quantum regime and the quantum limit of plasmonic confinement. **a**, Plasmonic interactions within the three regimes accessed in experiment. **b**, Near-field distributions for modes B → E from the QCM theory in each regime. Images are of 40 nm by 5 nm region, same intensity scale. **c**, The lateral confinement width w of each mode, extracted from the simulated near-field distribution, as the cavity width d is reduced. The dashed line marks the classical approximation $w = \sqrt{Rd}$. The onset of quantum tunnelling effects at $d = d_{QR} = 0.31$ nm sets a quantum limit (w_{QL}) on mode confinement in subnanometre plasmonic cavities.

METHODS SUMMARY

Experimental. Au-coated, ball-type AFM tips (150 nm radius of curvature) were obtained from Nanotools and used as received. Tips were mounted on separate three-axis piezoelectric actuation stages, axially aligned tip-to-tip at long range ($d > 50$ nm) using a nonlinear electrostatic-force technique[28], then brought together in 1-nm steps. Plasmons in the nanoscale cavity formed between the tip surfaces were excited with a supercontinuum laser tightly focused by a 0.9NA, 100× magnification objective in a dark field configuration. Scattered light was collected with the same objective and spatially filtered with a confocal pinhole to suppress background scattering. Spectral content of the scattered light was measured using a spectrometer with 3-ms integration time. Simultaneous electrical conductance measurements were taken by applying a submillivolt d.c. bias between the tips and measuring the resulting current.

Theoretical. Far-field scattering spectra and local-field distributions were calculated while reducing the inter-tip separation to identify the optical signature of tunnelling plasmonics and understand plasmon mode evolution through the quantum regime. Electron tunnelling effects were incorporated into a classical electrodynamics simulation using the QCM approach[15] to account for the quantum-mechanical tunnelling between particles. The tunnelling gap is described by a quantum-corrected dielectric function constructed from the full quantum-mechanical jellium calculation of the static gap conductivity. The optical response of the structure was then solved using a boundary-element method. Corresponding purely classical simulations were also performed.

Received 21 June; accepted 2 October 2012.
Published online 7 November 2012.

1. Xu, H., Bjerneld, E. J., Käll, M. & Börjesson, L. Spectroscopy of single hemoglobin molecules by surface enhanced Raman scattering. *Phys. Rev. Lett.* **83,** 4357–4360 (1999).
2. Schuck, P. J., Fromm, D. P., Sundaramurthy, A., Kino, G. S. & Moerner, W. E. Improving the mismatch between light and nanoscale objects with gold bowtie nanoantennas. *Phys. Rev. Lett.* **94,** 017402 (2005).
3. Cubukcu, E., Kort, E. A., Crozier, K. B. & Capasso, F. Plasmonic laser antenna. *Appl. Phys. Lett.* **89,** 093120 (2006).
4. Curto, A. G. *et al.* Unidirectional emission of a quantum dot coupled to a nanoantenna. *Science* **329,** 930–933 (2010).
5. Atwater, H. A. & Polman, A. Plasmonics for improved photovoltaic devices. *Nature Mater.* **9,** 205–213 (2010).
6. Nordlander, P., Oubre, C., Prodan, E., Li, K. & Stockman, M. I. Plasmon hybridization in nanoparticle dimers. *Nano Lett.* **4,** 899–903 (2004).
7. Romero, I., Aizpurua, J., Bryant, G. W. & de Abajo, F. J. G. Plasmons in nearly touching metallic nanoparticles: singular response in the limit of touching dimers. *Opt. Express.* **14,** 9988–9999 (2006).
8. Aubry, A., Lei, D. Y., Maier, S. A. & Pendry, J. B. Interaction between plasmonic nanoparticles revisited with transformation optics. *Phys. Rev. Lett.* **105,** 233901 (2010).
9. Prodan, E., Radloff, C., Halas, N. J. & Nordlander, P. A hybridization model for the plasmon response of complex nanostructures. *Science* **302,** 419–422 (2003).
10. Atay, T., Song, J.-H. & Nurmikko, A. V. Strongly interacting plasmon nanoparticle pairs: from dipole-dipole interaction to conductively coupled regime. *Nano Lett.* **4,** 1627–1631 (2004).
11. Jain, P. K., Huang, W. & El-Sayed, M. A. On the universal scaling behavior of the distance decay of plasmon coupling in metal nanoparticle pairs: a plasmon ruler equation. *Nano Lett.* **7,** 2080–2088 (2007).
12. Danckwerts, M. & Novotny, L. Optical frequency mixing at coupled gold nanoparticles. *Phys. Rev. Lett.* **98,** 026104 (2007).
13. Lassiter, J. B. *et al.* Close encounters between two nanoshells. *Nano Lett.* **8,** 1212–1218 (2008).
14. Taylor, R. W. *et al.* Precise subnanometer plasmonic junctions for SERS within gold nanoparticle assemblies using cucurbit[*n*]uril glue. *ACS Nano* **5,** 3878–3887 (2011).
15. Esteban, R., Borisov, A. G., Nordlander, P. & Aizpurua, J. Bridging quantum and classical plasmonics. *Nature Commun.* **3,** 825 (2012).
16. Novotny, L. & van Hulst, N. Antennas for light. *Nature Photon.* **5,** 83–90 (2011).
17. Scholl, J. A., Koh, A. L. & Dionne, J. A. Quantum plasmon resonances of individual metallic nanoparticles. *Nature* **483,** 421–427 (2012).
18. Ciracì, C. *et al.* Probing the ultimate limits of plasmonic enhancement. *Science* **337,** 1072–1074 (2012).

19. Zuloaga, J., Prodan, E. & Nordlander, P. Quantum description of the plasmon resonances of a nanoparticle dimer. *Nano Lett.* **9,** 887–891 (2009).
20. Song, P., Nordlander, P. & Gao, S. Quantum mechanical study of the coupling of plasmon excitations to atomic-scale electron transport. *J. Chem. Phys.* **134,** 074701 (2011).
21. Kern, J. *et al.* Atomic-scale confinement of resonant optical fields. *Nano Lett.* http://dx.doi.org/10.1021/nl302315g (published online 17 September 2012).
22. Duan, H., Fernández-Domínguez, A. I., Bosman, M., Maier, S. A. & Yang, J. K. W. Nanoplasmonics: classical down to the nanometer scale. *Nano Lett.* **12,** 1683–1689 (2012).
23. Bragas, A. V., Landi, S. M. & Martínez, O. E. Laser field enhancement at the scanning tunneling microscope junction measured by optical rectification. *Appl. Phys. Lett.* **72,** 2075–2077 (1998).
24. Schneider, N. L., Schull, G. & Berndt, R. Optical probe of quantum shot-noise reduction at a single-atom contact. *Phys. Rev. Lett.* **105,** 026601 (2010).
25. Chen, C., Bobisch, C. A. & Ho, W. Visualization of Fermi's golden rule through imaging of light emission from atomic silver chains. *Science* **325,** 981–985 (2009).
26. Ward, D. R., Hüser, F., Pauly, F., Cuevas, J. C. & Natelson, D. Optical rectification and field enhancement in a plasmonic nanogap. *Nature Nanotechnol.* **5,** 732–736 (2010).
27. Johansson, P. Light emission from a scanning tunneling microscope: fully retarded calculation. *Phys. Rev. B* **58,** 10823–10834 (1998).
28. Savage, K. J., Hawkeye, M. M., Soares, B. F. & Baumberg, J. J. From microns to kissing contact: dynamic positioning of two nano-systems. *Appl. Phys. Lett.* **99,** 053110 (2011).
29. Cappella, B. & Dietler, G. Force distance curves by atomic force microscopy. *Surf. Sci. Rep.* **34,** 1–104 (1999).
30. Ittah, N. & Selzer, Y. Electrical detection of surface plasmon polaritons by $1G_0$ gold quantum point contacts. *Nano Lett.* **11,** 529–534 (2011).

Supplementary Information is available in the online version of the paper.

Acknowledgements This work was supported by EPSRC grants EP/G060649/1 and EP/H007024/1, EU grant CUBi-HOLE, and projects FIS2010-19609-C02-01 and EUI200803816 from the Spanish Ministry of Science and Innovation. J.J.B. also acknowledges support from the Ikerbasque Foundation, Jesus College Cambridge and the University of Cambridge, and M.M.H. acknowledges support from a Canadian NSERC post-doctoral fellowship.

Author Contributions J.J.B. conceived of and planned the experiments. K.J.S. and M.M.H. designed, constructed and performed the experiments. J.A., A.G.B. and R.E. conceived of the theoretical approach, and carried out the calculations. All the authors contributed to analysing the results and writing the paper.

Author Information Reprints and permissions information is available at www.nature.com/reprints. The authors declare no competing financial interests. Readers are welcome to comment on the online version of the paper. Correspondence and requests for materials should be addressed to J.J.B. (jjb12@cam.ac.uk).